Solvent-Thermal Induced Roughening: a Novel and Versatile Method to Prepare Superhydrophobic Membranes

Weihua Qing [a], Xiaonan Shi [a], Weidong Zhang [b], Jianqiang Wang [a], Yifan Wu [a], Peng Wang [c], Chuyang Y. Tang [a,]*

a. Department of Civil Engineering, The University of Hong Kong, Pokfulam, Hong Kong 999077

b. State Key Laboratory of Chemical Resource Engineering, Beijing Key Laboratory of Membrane Science and Technology, Beijing University of Chemical Technology, Beijing 100029, People's Republic of China

c. Water Desalination and Reuse Center, Division of Biological and Environmental Sciences and Engineering, King Abdullah University of Science and Technology, Thuwal 23955-6900, Saudi Arabia

Abstract: Surface roughness enhancement by fabricating multi-scale nano/microstructure is an effective strategy to prepare superhydrophobic membranes. Here we report a novel solvent-thermal induced roughening (STIR) method. The method involves the swelling of a polymer surface to create a soft shell/hard core structure under the combined action of solvent and heating, followed by a controllable surface roughening as a result of mismatched thermal expansion between the shell and the core. We show a significant increase of surface roughness for a STIR-treated polyvinylidene fluoride nanofibrous membrane, whose nanofibers were covered with densely-packed nanofins. The treated membrane had greatly enhanced hydrophobicity, resulting in improved anti-wetting performance to low-surface-tension feed water in a membrane distillation process. The STIR method was capable of treating membranes with various pore structures. The novel surface roughening strategy opens up new directions to fabricate superhydrophobic surfaces and membranes, which can greatly benefit a wide range of applications such as membrane distillation, oil/water separation.

Keywords: surface roughness enhancement, solvent-thermal treatment, superhydrophobic

membrane, polyvinylidene fluoride, membrane distillation

1. Introduction

Superhydrophobic membranes, characterized by water contact angles of greater than 150 °, have attracted growing interests [1–3] not only for fundamental research but also for its wide range of applications (e.g., oil/water separation [4], battery and fuel cells [5,6], CO_2 capture [7], and membrane distillation [8–10]). Generally, the wettability of the membrane is related to its surface energy and surface roughness. According to the Cassie–Baxter theory, low surface energy alone is often insufficient to achieve superhydrophobicity, as it requires in addition a desired surface roughness [11]. Over the past decades, researcher have devoted to the fabrication of superhydrophobic membranes using appropriate combination of the two factors [12,13]. While the anti-wetting topping can be readily achieved by using hydrophobic membrane materials (e.g., polytetrafluoroethylene, polyvinylidene fluoride (PVDF) and polydimethylsiloxane) or by coating of low-surface-energy chemicals (alkanethiols, fluorinated alkanes, and fatty acids) [14,15], the challenge to create stable rough surfaces needs to be further addressed [16,17].

Strategies for enhancing roughness can be divided into two main groups [18] by either removing materials from or adding materials to a surface. Examples of the former approach include templating [19], lithography [20], and laser processing [21] that often involves complicated preparation procedures. For example, templating approach requires the preparation of templates with desired features, followed by molding, and finally lifting off or dissolving the templates to obtain the patterned structure [18]. Alternatively, surface roughness can be created by adding materials to an existing surface through self-assembly [22,23], chemical deposition [24], sol-gel

methods [25], aggregation of particles [26], etc. However, roughness structures created by these additive approaches are often unstable due to their potential detachment from the surface [11]. Thus, novel methods for preparing stable roughness structures are highly desirable.

Herein, we report a facile solvent-thermal induced roughening (STIR) method to manipulate the surface roughness of a membrane and thus its wetting behavior. As illustrated in Figure 1, we apply a solvent-thermal treatment to a polymeric membrane, during which a solvent is also added. The combined solvent and thermal treatment partially swells the polymer to form a soft-shell/hard-core structure (Figure 1a). The mismatched thermal expansion between the shell and the core folds the soft shell to create nano-structured surface wrinkles over polymeric materials. We show that higher surface roughness increases the hydrophobicity and surface area of the membrane to achieve a greatly improved anti-wetting performance in a membrane distillation (MD) process. We further demonstrate the versatility of the STIR method by creating roughness structures on various forms of polymeric substrates. The novel solvent-thermal strategy opens new directions to fabricate superhydrophobic surfaces and membranes.

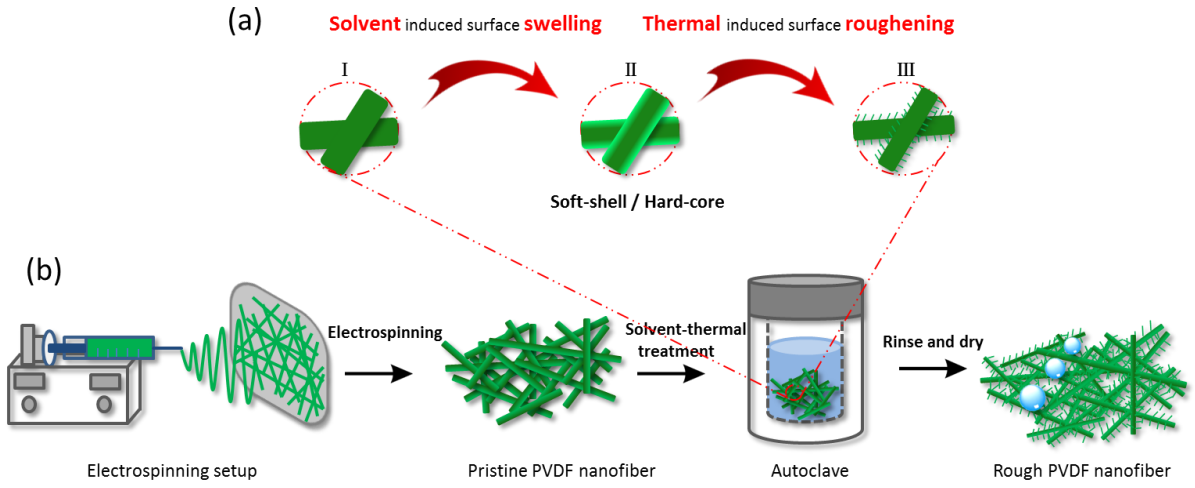

Figure 1. Schematic illustrasion of solvent-thermal induced roughening (STIR): (a) Mechanism of STIR; (b) fabrication process of superhydrophobic PVDF nanofibrous membrane. PVDF nanofibrous membranes are prepared by electrospinning. During the STIR treatment, a typical PVDF nanofiber (I) undergoes surface swelling to form a soft-shell/hard-core structure (II). The mismatched thermal expansion between the soft shell and the hard core induces

the formation of surface roughness (III).

2. Experimental Section

2.1 Materials

Poly(vinylidene fluoride) (PVDF) beads (average Mw ~180000) were purchased from Aldrich Chemical Inc.. Sodium dodecyl sulfate (SDS) was purchased from Uni-Chem Company. Sodium chloride, hydrogen chloride (HCl, 37wt.%), n-butanol, ethanol, and N,N-Dimethylformamide (DMF) were all purchased from VWR Chemicals Ltd.. All the chemicals were of ACS reagent grades and were used without further purification. Milli-Q water (Resistivity 18.2 MΩ.cm, TOC 2 ppb, Millipore, Billerica, MA) was used in this study.

2.2 Preparation of PVDF membranes

A 25 wt.% PVDF solution was first prepared by dissolving the polymer in DMF and stirring the mixture at 60 ^{o}C overnight. Three different types of PVDF membranes were prepared using the same polymer solution.

The nanofibrous membrane was prepared by electrospinning 15 mL of the polymer solution onto an aluminum foil mounted on a rotating drum. A pre-optimized electrospinning conditions were applied (see Figure S1): applied voltage = 24 kV, polymer solution flow rate = 0.88 mL/h, spinneret/collector distance = 15 cm, drum diameter = 10 cm, and drum rotating speed = 80 rpm.

For the preparation of PVDF membrane with microsphere morphology, a PVDF film was prepared by casing the PVDF solution on a clean glass plate at a casting gate height of 250 μm (Elcometer 4340 Automatic Film Applicator, UK). The glass plate was kept in a fume hood overnight to allow the volatile solvent to evaporate. After total solidification, the resultant PVDF membrane was peeled off from the glass plate for further use.

For the preparation of PVDF membrane with microsphere morphology, a freshly-casted PVDF film was first prepared on a clean glass plate using the same procedure above, and then immersed into a water (non-solvent) bath at the room temperature for phase inversion. The resultant membrane was peeled off from the glass plate and dried in an oven at 60 ^{o}C for 24 hours.

2.3 Solvent-thermal treatment

A solvent-thermal treatment solution was prepared in a Teflon-lined autoclave by adding HCl, Milli-Q water and n-butanol at a pre-optimized volume ratio of HCl : water : n-butanol = 15 mL : 15 mL : 0.54 mL (if not specifically stated). A piece of membrane (3 cm × 3 cm if not specifically stated) was then immersed into the solution. The solvent-thermal treatment was conducted at 150 ^{o}C in an electric oven for 4 hours. Afterwards, the membrane was rinsed with ethanol and Milli-Q water in an ultrasonic cleaner three times, before being dried in the electric oven at 60 ^{o}C overnight.

2.4 Direct-contact membrane distillation (DCMD) experiments

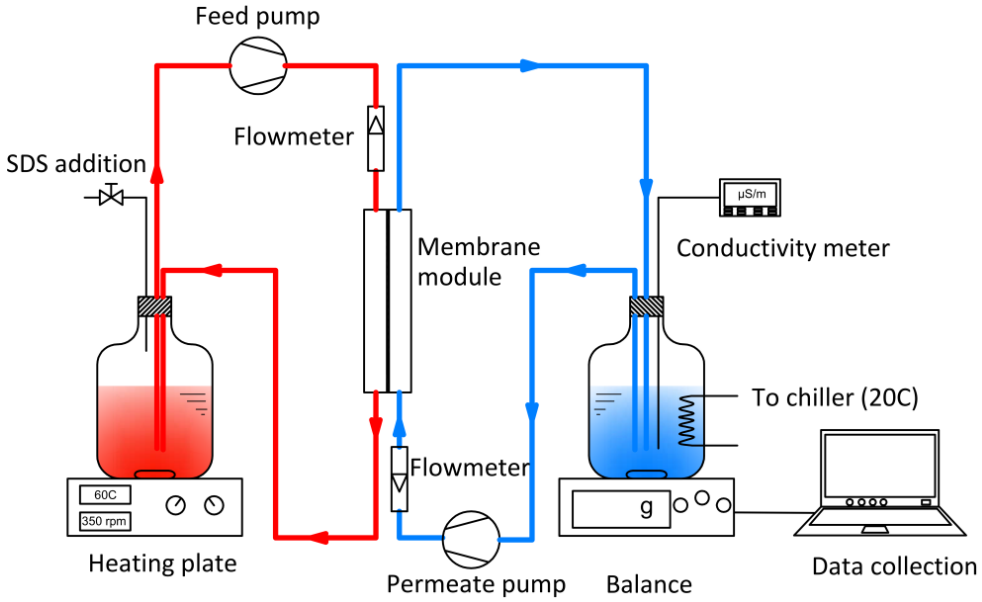

Figure 2 Schematic diagram for direct-contact membrane distillation setup

The desalination performances of the pristine and treated membranes were evaluated in a

custom-made DCMD setup (Figure 2). The effective membrane area was 9 cm^2 (1.5 cm × 6 cm), and all of the tubes were insulated to minimize the heat loss. The hot feed (60 ± 0.5 °) was initially filled with 1.5 L of a 3.5 wt.% NaCl solution. The permeate container with 0.5 L Milli-Q water (20 ± 0.5 °) was placed on an electronic balance that was connected to a computer. The feed and permeate solutions were circulated in counter-current directions at a flow rate of 0.44 L/min. The permeate conductivity was measured by a submerged conductivity probe, and the flux was calculated using the following equation:

$$J = \frac{\Delta m}{A \times \Delta t} \qquad (1)$$

where J is the flux, Δm is the weight increase of the permeate container over a time period of Δt, and A is the effective membrane area.

The DCMD experiment was conducted for an initial period of 2 hours using a 3.5% NaCl feed solution. Subsequently, sodium dodecyl sulfate (SDS) was added to the feed solution to evaluate the wetting resistance of the pristine and treated PVDF membranes. The following SDS concentrations of 0.05, 0.1, 0.15, 0.2 and 0.25 mM, increased sequentially at 2-hour time intervals, were adopted in the current study. The feed solution was replenished with Milli-Q water every 2 hours to maintain variation of SDS concentration within 1 %.

2.5 Characterization

Scanning electron microscope (SEM) and transmission electron microscopy (TEM) were used to characterize the membrane morphology. SEM characterization was conducted using a Field Emission Gun Scanning Electron Microscope (LEO1530 FEG SEM, UK) at an accelerating voltage of 5 kV. Mean diameter of nanofibers was measured via SEM image analysis (Nano Measure System, 1.2). TEM sample characterization was performed with Philips CM100 TEM (Philips,

Eindhoven, Netherlands) operating at 100 kV. The average surface roughness of the nanofiber was measured by an atomic force microscope (AFM, JPK Instruments AG, Berlin, Germany). In each case, an area of 5 μm × 5 μm was scanned using the tapping mode, and the average surface roughness (R_a) for a single nanofiber was calculated from the roughness profile determined by AFM.

To reveal the chemical composition variation during the STIR treatment process, the pristine and treated PVDF nanofibrous membranes were characterized by X-ray photoelectron spectroscopy (XPS) using a spectrometer (Thermo Fisher Scientific, ESCALAB250) with an X-ray source of monochromic Al Kα 150W. Water static contact angle (SCA) measurements were performed using Kruss DSA 100 (Kruss GmbH, Hamburg, Germany). Each deionized water droplet with a volume of approximately 6 μL was introduced to the membrane surface, and a stabilizing time of approximate 10 s was allowed. Water sliding angle was measured using a goniometer (Suruga Seiki, Japan). For each membrane types, the values reported were the average of the contact angles obtained at six different locations. Membrane thickness was measured by a Digital Calipers. For each membrane sample, thickness was measured at five different locations, and the average value was reported. Surface area measurements were carried out using the BET nitrogen adsorption method with a Micromeritics TriStar II 3020 instrument at 77 K, after pretreating the samples overnight under vacuum at 90 ^{o}C. For calculation of the BET specific surface area, relative pressures in the range of 0.05–0.2 were used.

The Liquid entry pressure (LEP) of the membrane was measured a capillary flow porometer (POROLUX™ 1000, Germany). First, a membrane sample was sealed in a chamber of the porometer, after which distilled water was filled in chamber to cover the membrane surface. Then a

pressure was applied in the chamber by increasing N_2 gas at a rate of 20 s/bar. The appearance of a pressure increase at the permeate side of the chamber was taken as the LEP of the membrane.

Pososity of the membrane was obtained by gravimethic method. First, the dry weight of membrane samples were measured before they were immersed into isopropyl alcohol (IPA). After 8 hours of immersion, the samples were carefully taken out, and the wet membrane were measured after IPA on the membrane surfaces were carefully removed by lab wipers. The membrane porosity could be calculated by the following equation:

$$\varepsilon = \frac{(\omega_1 - \omega_2)/D_i}{(\omega_1 - \omega_2)/D_i + \omega_2/D_p} \quad (2)$$

Where is ω_1 the weight of the wet membrane, g; ω_2 is the weight of dry membrane, g; D_i is the IPA density, 7.68×10^5 g/m^3; D_P is the density of PVDF, 17.8×10^5 g/m^3. Two measurements were performed for each membrane sample and the average values were reported.

3. Results and Discussion

3.1 Morphology and chemical composition

In a typical example, we fabricated a superhydrophobic PVDF nanofibrous membrane with high roughness using the STIR method (Figure 1b). A pristine PVDF nanofibrous membrane was first prepared by electrospinning, a technique that is commonly used to prepare highly porous membranes with controllable thickness and pore size [15]. The membrane was immersed in a Teflon-lined autoclave containing a treatment solution (water, hydrochloric acid and n-butanol) and hydrothermally treated at 150 ^{o}C for 4 hours. The morphology and roughness of the resulting membrane and its wetting behavior were characterized.

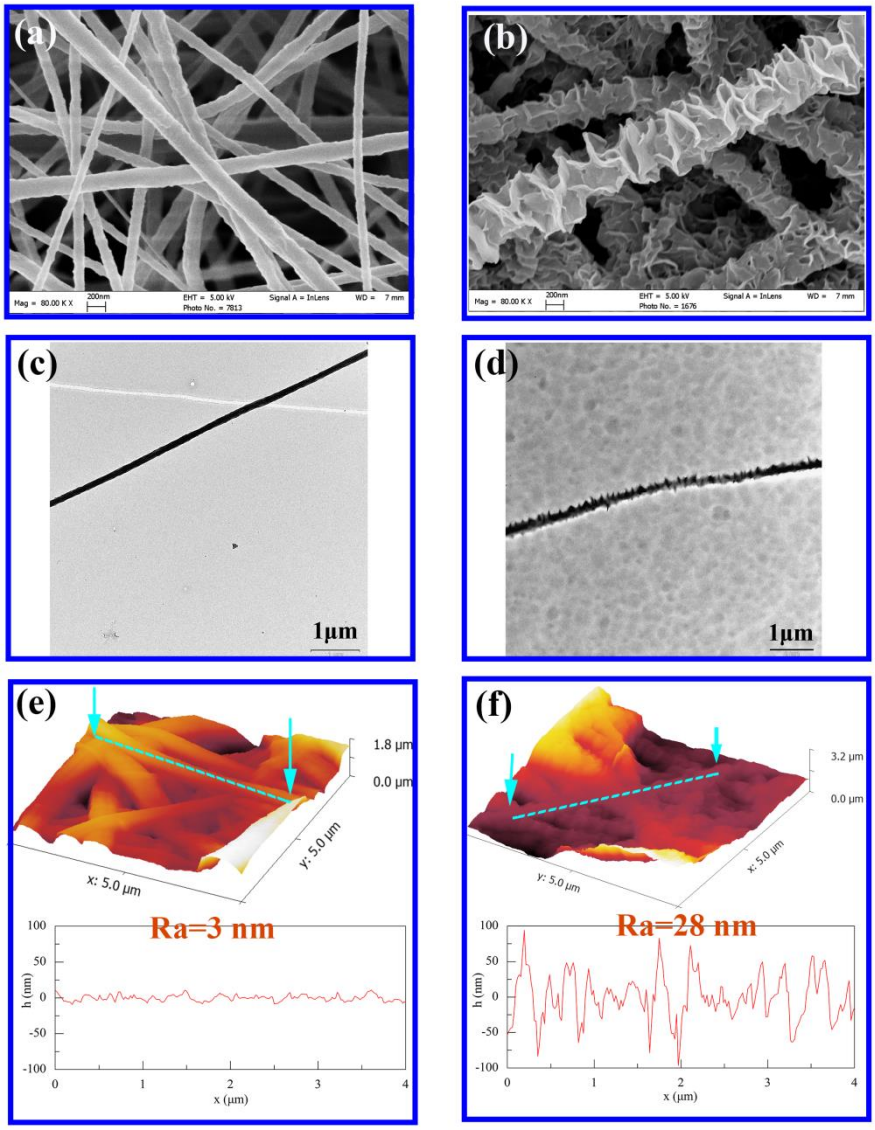

Figure 3. Surface morphology and chemical composition of PVDF nanofibrous membranes: SEM images of pristine (a) and solvent-thermal treated (b) PVDF nanofibrous membranes; TEM images of pristine (c) and solvent-thermal treated (d) PVDF nanofibrous membranes; AFM 2D and 3D images of pristine (e) and solvent-thermal treated (f) PVDF nanofibrous membrane, where R_a represents the average roughness of a single nanofiber measured along the marked line. Solvent-thermal treatment conditions: HCl:water:n-butanol=15mL:15mL:0.54mL, 150 ^{o}C, 4 hours.

Table 1 Characteristics of the pristine and treated PVDF membranes

Types	Mean fiber diameter (nm)	Porosity (%)	Mean pore size (nm)	BET surface area (m^2/g)	Thickness (mm)	Tensile strength (MPa)
Pristine	257±33	89.2±1.3	908.8±5.4	7.3	0.18±0.02	2.5±0.3
Treated	681±93	67.7±0.4	127.0±7.7	19.0	0.29±0.01	2.6±0.5

Figure 3 shows the morphologies of the PVDF nanofibrous membranes. The pristine

electrospun PVDF nanofibrous membrane had a three-dimensional porous structure, with a mean nanofiber diameter of 257 nm (Figure 3a and Table 1). Transmission electron microscopy (TEM) revealed a smooth surface of the as-spun nanofibers (Figure 3c). Atomic force micrograph (AFM) further showed that the average roughness for a typical pristine nanofiber was merely 3 nm. However, after a STIR treatment at 150 ^{o}C for 4 h, a highly rough nanofiber was obtained. SEM (Figure 3b) characterization shows a corrugated nanostructure with a densely-packed array of fin-like features that were perpendicular to the nanofiber. TEM image of the treated nanofiber further revealed a rough-surface-on-hard-core morphology (Figure 3d). Compared to the pristine nanofibers, the mean diameter of the STIR treated ones increased to 681 nm (Table 1), which can be attributed by the combined effects of swelling and roughness formation. AFM characterization confirmed that the average roughness for a typical treated nanofiber increased significantly to 28 nm, which is approximately one order of magnitude larger than that of the pristine nanofiber (Figure 3e,f). The densely-packed nanofin structure on the treated PVDF membrane also greatly increased the BET surface area from 7.3 to 19.0 m^2/g (Table 1). However, the mean pore size and porosity were both decreased (Table 1) due to the membrane shrank after the STIR treatment, which could adversely affect the membrane permeability (see further discussion in Section 3.3).

X-ray photoelectron spectroscopy (XPS) survey spectra (Figure 4) show similar atomic composition for the pristine and treated PVDF nanofibers. For both samples, only carbon and fluorine were detected at an C/F ratio of 1.0, which is consistent to the molecular structure of PVDF ($[C_2H_2F_2]_n$) noting that XPS does not detect H. This result suggests that the roughening of the nanofiber was caused by physical changes instead of chemical modification.

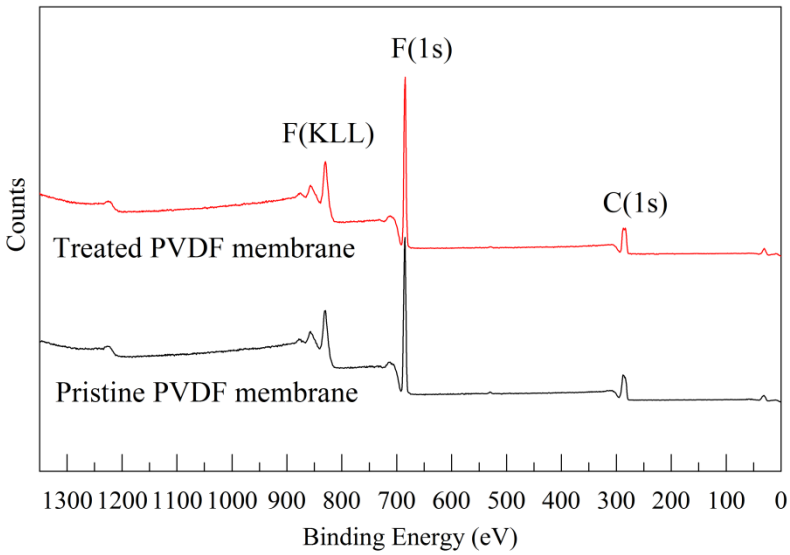

Figure 4. XPS survey spectra for PVDF membranes before and after solvent-thermal treatment.

To better understand the formation process of the rough structure, we further investigated the effects of n-butanol, HCl, treatment temperature, and treatment duration (Figure S2-5, Supporting Information, SI) on the nanofiber morphology. When n-butanol was not added, the characteristic corrugated rough structure could not form after the solvent-thermal treatment (Figure S2, SI). This result reveals the critical role of the solvent for the roughness formation. Without the presence of n-butanol, the inherently hydrophobic PVDF nanofibers can hardly be swelled by the aqueous solution, which prevents the formation of the soft-shell/hard-core structure and therefore suppresses the mismatch in thermal expansion. The treatment temperature is another key parameter for the creation of the rough structure. As shown in Figure S4 (SI), the corrugated rough structure did not form at 120 ^{o}C, which underscores the critical role of treatment temperature. A higher temperature causes greater swelling of the soft shell as well as induces greater thermal stress; both conditions favor the roughening of the membrane surface. However, overly excessive thermal treatment (e.g., a high treatment temperature of 170 ^{o}C (Figure S4, SI) or a long treatment duration of 8 h (Figure S5, SI), the nanofiber backbone was destroyed as a result of severe membrane deformation.

On the basis of the analysis above, a possible mechanism for the creation of nanofin structures on the PVDF nanofiber is proposed (Figure 1a): The outer skin of the nanofiber is swelled under the combined action of solvent and heating. At the same time, the inner core is less affected as it is not readily accessible by the solvent. Consequently, a transitional soft-shell/hard-core structure is formed. The anisotropic swelling induces mismatched internal stress in the nanofiber, which offers a driving force for macroscopic deformation between the shell and the core. With the treatment proceeds, the soft shell is folded under the internal stress to create nanofins over the nanofibers.

3.2 Wettability

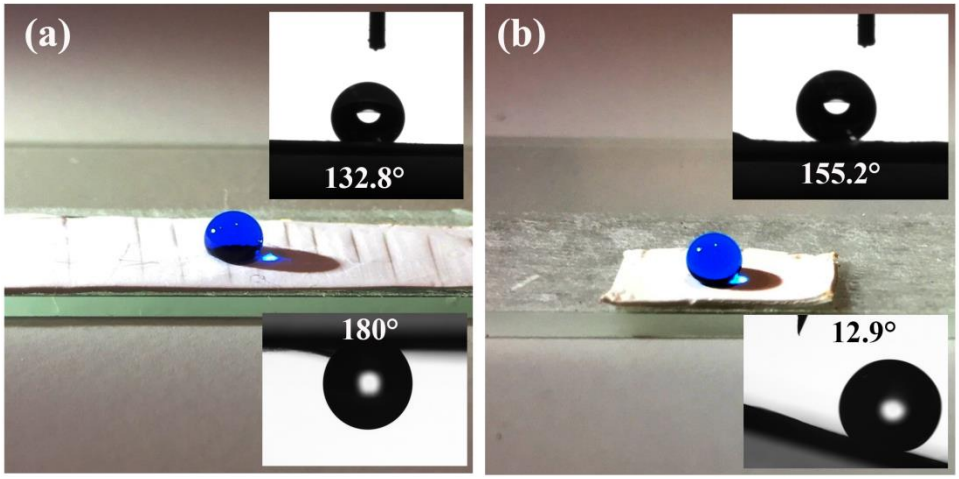

Figure 5. Photos of water droplet on a pristine (a) or solvent-thermal treated (b) PVDF nanofibrous membrane, insets on top and lower right corner of both images show the water contact angle and sliding angle measurements, respectively.

Table 2 Wettability of the pristine and treated PVDF membranes

Types	Water contact angle (°)	Water sliding angle (°)	SDS contact angle [a] (°)	LEP (kPa)
Pristine	132.8±3.4	180	108.7±7.8	83±3
Treated	155.2±0.2	12.9	144.9±2.5	325±8

[a] Contact angle with 3.5 wt % NaCl solution containing 0.05 mM SDS.

The wetting behaviors of the membranes are presented in Figure 5 and Table 2. The pristine PVDF membrane had a water contact angle of 132.8 °(Figure 5a). When the membrane was placed upside down, the water droplet still pinned on the membrane surface (inset in Figure 5a). This

observation revealed that the wetting behavior of water on the pristine PVDF membrane surface may be governed by the Wenzel state, in which the water droplet can fully wet the membrane surface [27].

The STIR treated membrane had an increased contact angle of 155.2 °(Figure 5b), indicating a superhydrophobic property of the membrane was obtained. Moreover, this membrane surface was non-sticky to water and the sliding angle of water droplet decreased significantly to only 12.9 °. Additionally, the SDS contact angle of the treated membrane was higher than that of pristine membrane (Table 2), showing an superior wetting resistance of the treated membrane towards low-surface-tension liquid. The combination of low sliding angle and large contact angle confirms a greatly improved anti-wetting property of the treated nanofibrous membrane, which may result from a transition of wetting behavior from the Wenzel regime to the Cassie-Baxter regime [12]. The corrugated rough structure of the treated membrane can allow a water droplet to roll over the nanofins on its surface without occupying the voids between them. Consequently, the air packets trapped underneath the water droplet increases hydrophobicity and water mobility on the membrane surface [13].

3.3 Anti-wetting performance in DCMD

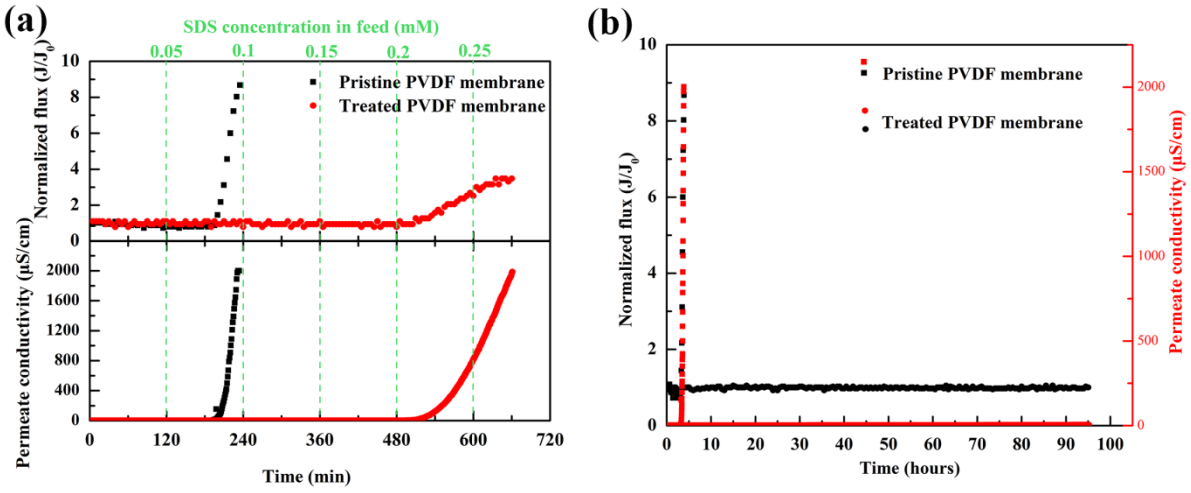

Figure 6 Anti-wetting performance of the pristine and treated PVDF membranes in DCMD: (a) Normalized flux (upper panel) and permeate conductivity (lower panel) using 3.5 wt.% NaCl at 60 ^{o}C with varying SDS concentration as feed solution and water at 20 ^{o}C as permeate stream. Initial fluxes for the pristine and treated membranes were 18 and 9 Kg/m^{2}h, respectively, and were calculated as an average value of the first 30 min of experiments. (b) Long time duration of the membranes in DCMD using 3.5 wt.% NaCl at 60 ^{o}C with 0.05 mM SDS concentration as feed solution and water at 20 ^{o}C as permeate stream. The STIR treatment conditions for membranes used for DCMD experiments: HCl:water:n-butanol=90mL:90mL:3.24mL, 150 ^{o}C, 4 hours, pristine membrane area: 9cm×16cm.

Nowadays, water crisis has been recognized as a global concern and increasing interests have been paid to convert seawater to potable water by membrane distillation (MD). MD desalination is driven by a vapor pressure gradient existing between a porous hydrophobic membrane, and vapor from the hot feed side transports through the porous membrane to the cold permeate side, while the nonvolatile components are retained by the membrane [28]. However, wetting of MD membranes, which compromise their salt rejection, remains as a critical challenge [29].

We demonstrate improved anti-wetting performance for the STIR treated membrane in MD process [9,10,30]. In our DCMD experiments, a synthetic seawater (3.5 wt.% NaCl at 60 ^{o}C) was used as the feed water, and an anionic surfactant (sodium dodecyl sulfate, SDS) was dosed in the feed water to accelerate the wetting process. The concentration of SDS was ramped from 0 to 0.25 mM by dosing additional SDS every 2 h. As shown in Figure 6a, both the pristine membrane and treated membrane showed stable desalination performance without the addition of SDS. The normalized flux showed almost no changes and the conductivity of permeate remained at around 1.1 μS/cm. A higher initial flux of the pristine membrane (18 *vs.* 9 Kg/m^{2}h) was observed, which can be attributed to its higher porosity (89% *vs.* 68%) and larger mean pore size (908.8 *vs.* 127.0 nm) when compared to the treated membrane (see Table 1). However, the pristine membrane experienced a dramatic increase in the water flux and permeate conductivity shortly after the dosage of 0.05 mM SDS. Visual inspection showed that parts of the membrane turned from opaque to

translucent (Figure S6b, SI). These results suggest that the pristine membrane had been wetted at an SDS concentration of merely 0.05 mM.

The treated PVDF membrane showed stable flux and permeate conductivity at 0.05 mM SDS over a 96 h operation (Figure 6b), and the membrane did not exhibit any visible signs of wetting (Figure S6d, SI). Upon further increasing the SDS concentration in the feed, the membrane maintained stable performance for SDS concentrations up to 0.15 mM (Figure 6a). Membrane wetting occurred only after 0.2 mM SDS addition. These results demonstrated that the treated membrane offered a superior wetting resistance to the low-surface-tension feed water than the pristine membrane. This enhanced anti-wetting performance could be attributed to the enhanced hydrophobicity of the treated membrane by creating a secondary perpendicularly-arrayed nanofin structure. The enhanced anti-wetting performance of the treated membrane is also reflected by its greatly increased liquid entry pressure (325 kPa of the treated membrane vs. 83 kPa of the pristine membrane, see Table 2).

3.4 Versatility of STIR method

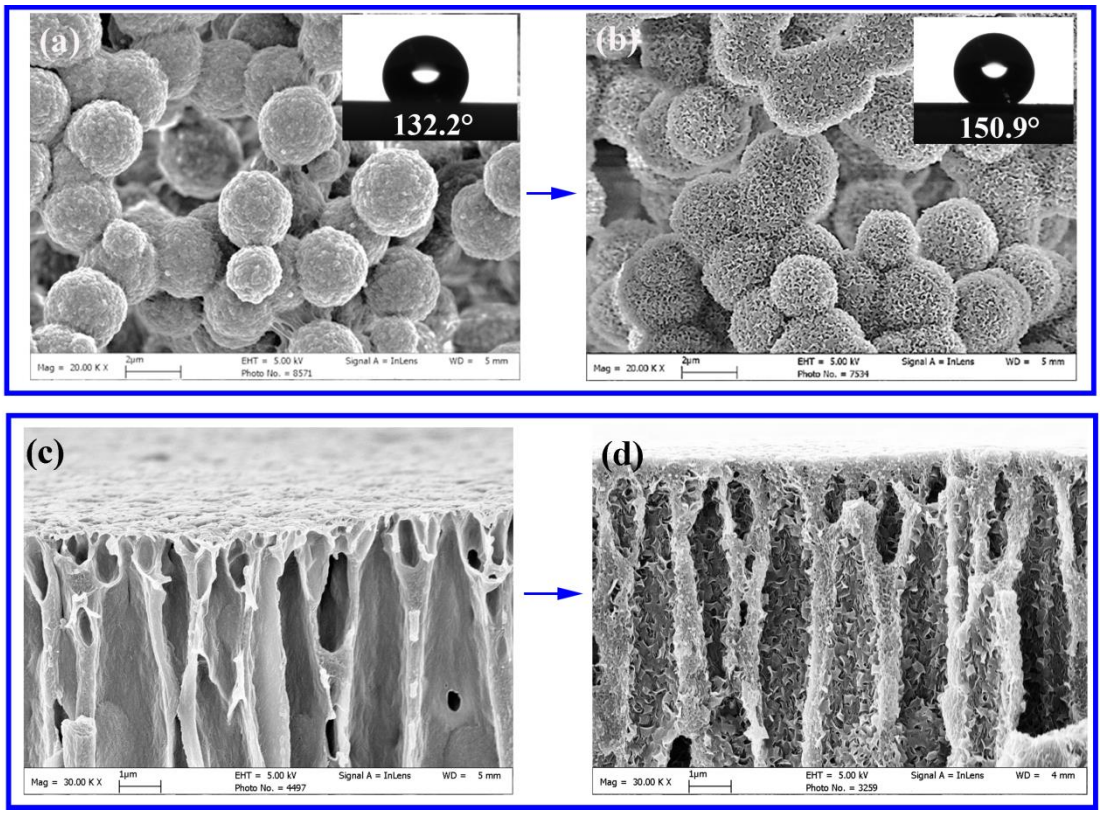

Figure 7. Morphology of the PVDF membranes. a-b), SEM images of pristine and treated PVDF membranes with stacked-microsphere morphology, respectively. Insets on the top right corner shows the water contact angle measurement. Solvent-thermal treatment conditions: HCl:water:n-butanol=15mL:15mL:0.54mL, 150 ^{o}C, 4 hours. c-d), SEM images of the pristine and treated PVDF membrane with finger-like pore morphology, respectively. Solvent-thermal treatment conditions:: HCl:water:n-butanol=15mL:15mL:1.08mL, 150 ^{o}C, 4 hours.

We further demonstrate the versatility of the STIR method by creating nanofin-like rough structures on membranes with alternative pore structures (stacked-microsphere and finger-like pore structures, Figure 7). The STIR treatment of microspheres greatly roughened their surfaces to form a flower-like morphology. TEM images of the treated microsphere further revealed a rough-surface-on-hard-core morphology in contrast to the more uniform structure of the pristine membrane (Figure 7, SI). Corresponding to the surface roughening, the water contact angle increased from 132.2 ° (the pristine membrane) to 150.9 ° (the treated membrane). Alternatively, we applied the STIR treatment to a membrane with finger-like pore structure, which resulted in nanofin coverage throughout the pore channels. Moreover, these “finger-like” pore channels were not

destroyed by the treatment process, indicating that STIR is a controllable surface modification method.

4. Conclusions

In conclusion, we have developed a novel and versatile STIR method to increase roughness on various membrane surfaces for enhanced hydrophobicity. The treatment involves the swelling of a polymer surface to create a soft shell/hard core structure under the combined action of solvent and heating, followed by a controllable surface roughening as a result of thermal-induced deformation of the soft shell. A highly rough PVDF nanofibrous membrane was prepared based on this method. Corrugated nanofin structures were formed on the nanofibers after STIR treatment, which increased the average roughness of one typical nanofiber from 3 nm to 28 nm. The resulting membrane, with a water contact angle of 155.2°, showed superior anti-wetting performance to the low-surface-tension feed water than the pristine one in membrane distillation application. We further demonstrated the applicability of the method to membranes with distinctly different pore structures. The novel solvent-thermal strategy reported here opens up new directions to fabricate superhydrophobic surfaces and membranes, which can greatly benefit a wide range of applications such as membrane distillation, oil/water separation.

Supporting Information

Supporting Information is available from the Online Library or from the author.

Acknowledgements

This publication is based upon work supported by the King Abdullah University of Science

and Technology (KAUST) Office of Sponsored Research (OSR) under Award No. OSR-2017-CPF-3320. The authors also acknowledge the partial financial support from the NSFC/RGC Joint Research Scheme sponsored by the Research Grants Council of Hong Kong and the National Natural Science Foundation of China (N_HKU706/16).

Conflict of Interest

The authors declare no conflict of interest.

References:

[1] H. Mertaniemi, V. Jokinen, L. Sainiemi, S. Franssila, A. Marmur, O. Ikkala, et al., Superhydrophobic Tracks for Low-Friction, Guided Transport of Water Droplets, Adv. Mater. 23 (2011) 2911–2914.

[2] R.B. Pernites, R.R. Ponnapati, R.C. Advincula, Superhydrophobic-Superoleophilic Polythiophene Films with Tunable Wetting and Electrochromism, Adv. Mater. 23 (2011) 3207–3213.

[3] X. Yao, Y. Song, L. Jiang, Applications of Bio-Inspired Special Wettable Surfaces, Adv. Mater. 23 (2011) 719–734.

[4] W. Qing, X. Shi, Y. Deng, W. Zhang, J. Wang, C.Y. Tang, Robust superhydrophobic-superoleophilic polytetrafluoroethylene nanofibrous membrane for oil/water separation, J. Memb. Sci. 540 (2017) 354-361.

[5] S. Han, D. Wu, S. Li, F. Zhang, X. Feng, Porous Graphene Materials for Advanced Electrochemical Energy Storage and Conversion Devices, Adv. Mater. 26 (2014) 849–864.

[6] V.A. Lifton, S. Simon, Robust Si-Based Membranes for Fluid Control in Microbatteries Using Superlyophobic Nanostructures, J. Microelectromechanical Syst. 20 (2011) 73–82.

[7] F. Geyer, C. Schönecker, H.-J. Butt, D. Vollmer, Enhancing CO_2 Capture using Robust Superomniphobic Membranes, Adv. Mater. 29 (2017) 1-6.

[8] A.P. Straub, N.Y. Yip, S. Lin, J. Lee, M. Elimelech, Harvesting low-grade heat energy using thermo-osmotic vapour transport through nanoporous membranes, Nat. Energy. 1 (2016) 1-6.

[9] P.D. Dongare, A. Alabastri, S. Pedersen, K.R. Zodrow, N.J. Hogan, O. Neumann, et al., Nanophotonics-enabled solar membrane distillation for off-grid water purification., Proc. Natl. Acad. Sci. U. S. A. 114 (2017) 6936–6941.

[10] A. V. Dudchenko, C. Chen, A. Cardenas, J. Rolf, D. Jassby, Frequency-dependent stability of CNT Joule heaters in ionizable media and desalination processes, Nat. Nanotechnol. 12 (2017) 557–563.

[11] X. Tian, T. Verho, R.H.A. Ras, Moving superhydrophobic surfaces toward real-world applications, Science (80-.). 352 (2016) 142–143.

[12] P. Ragesh, V. Anand Ganesh, S. V. Nair, A.S. Nair, A review on "self-cleaning and multifunctional materials," J. Mater. Chem. A. 2 (2014) 14773-14797.

[13] Z. Xue, Y. Cao, N. Liu, L. Feng, L. Jiang, Special wettable materials for oil/water separation, J. Mater. Chem. A. 2 (2014) 2445–2460.

[14] X. Zhang, F. Shi, J. Niu, Y. Jiang, Z. Wang, D.O.H. Teare, et al., Superhydrophobic surfaces: from structural control to functional application, J. Mater. Chem. 18 (2008) 621–633.

[15] N. Nuraje, W.S. Khan, Y. Lei, M. Ceylan, R. Asmatulu, Superhydrophobic electrospun nanofibers, J. Mater. Chem. A. 1 (2013) 1929–1946.

[16] A. Gao, Q. Wu, D. Wang, Y. Ha, Z. Chen, P. Yang, A Superhydrophobic Surface Templated by Protein Self-Assembly and Emerging Application toward Protein Crystallization, Adv. Mater. 28 (2016) 579–587.

[17] T. Darmanin, E.T. de Givenchy, S. Amigoni, F. Guittard, Superhydrophobic Surfaces by Electrochemical Processes, Adv. Mater. 25 (2013) 1378–1394.

[18] X.-M. Li, D. Reinhoudt, M. Crego-Calama, A.J.H. Suurmeijer, W. Timens, I. Stokroos, et al., What do we need for a superhydrophobic surface? A review on the recent progress in the preparation of superhydrophobic surfaces, Chem. Soc. Rev. 36 (2007) 1350-1368.

[19] M. Suwan, M. Jaleh, Y. Yun, C. Vicki, Effect of templating agents on the properties and membrane distillation performance of TiO2-coated PVDF membranes, J. Memb. Sci. 450 (2014) 48–59.

[20] M. Im, H. Im, J. Lee, J. Yoon, Y. Choi, A robust superhydrophobic and superoleophobic surface with inverse-trapezoidal microstructures on a large transparent flexible substrate, Soft Matter. (2010) 1401-1404.

[21] F. J., C. J.P., P.-E. F., Synthesis of transparent superhydrophobic polyethylene surfaces, Surf. Coatings Technol. 200 (2006) 5296–5305.

[22] J. Yuan, X. Liu, O. Akbulut, J. Hu, S.L. Suib, J. Kong, et al., Superwetting nanowire membranes for selective absorption, Nat. Nanotechnol. 3 (2008) 332–336.

[23] T. Ogawa, B. Ding, Y. Sone, S. Shiratori, Super-hydrophobic surfaces of layer-by-layer structured film-coated electrospun nanofibrous membranes, Nanotechnology. 18 (2007) 165607.

[24] L. Zhang, B. Tang, J. Wu, R. Li, P. Wang, Hydrophobic Light-to-Heat Conversion Membranes with Self-Healing Ability for Interfacial Solar Heating, Adv. Mater. 27 (2015) 4889–4894.

[25] A. N.A., L. C.P., A. A.L., Synthesis of superhydrophobic alumina membrane: Effects of sol–gel coating, steam impingement and water treatment, Appl. Surf. Sci. 284 (2013) 556–564.

[26] L.-B. Lv, T.-L. Cui, B. Zhang, H.-H. Wang, X.-H. Li, J.-S. Chen, Wrinkled Graphene Monoliths as Superabsorbing Building Blocks for Superhydrophobic and Superhydrophilic Surfaces, Angew. Chemie. 127 (2015) 15380–15384.

[27] H.F. Hoefnagels, D. Wu, G. de With, W. Ming, Biomimetic Superhydrophobic and Highly

Oleophobic Cotton Textiles, Langmuir. 23 (2007) 13158–13163.

[28] D.M. Warsinger, J. Swaminathan, E. Guillen-Burrieza, H.A. Arafat, J.H. Lienhard V, Scaling and fouling in membrane distillation for desalination applications: A review, Desalination. 356 (2015) 294–313.

[29] M. Khayet, Membranes and theoretical modeling of membrane distillation: A review, Adv. Colloid Interface Sci. 164 (2011) 56–88.

[30] A. Alkhudhiri, N. Darwish, N. Hilal, Membrane distillation: A comprehensive review, Desalination. 287 (2012) 2–18.